Obacunone inhibits ferroptosis through regulation of Nrf2 homeostasis to treat diabetic nephropathy

YI OU[1] and WENJUAN ZHANG[2]

[1]Department of Endocrinology, Shenzhen Fuyong People's Hospital, Shenzhen, Guangdong 518100, P.R. China; [2]Department of Public Health and Preventive Medicine, School of Basic Medicine, Jinan University, Guangzhou, Guangdong 510000, P.R. China

Received October 16, 2024; Accepted January 23, 2025

DOI: 10.3892/mmr.2025.13500

Abstract. Diabetic nephropathy (DN), a prevalent and severe microvascular complication of diabetes, often leads to end-stage renal disease and poses a threat to patient survival. However, to the best of our knowledge, there are currently no effective strategies available for the treatment of DN. Obacunone (OB), a small-molecule natural compound derived from *Citrus* plants, exhibits various pharmacological effects; however, the impact of OB on DN remains to be fully elucidated. Therefore, the present study aimed to explore the effects and potential mechanisms of OB in DN. In the current study, DN models were created *in vitro* by treating HK-2 cells with high-glucose (HG) levels, and *in vivo* by administering a HG and high-fat diet along with intraperitoneal injections of streptozotocin to Sprague-Dawley rats. Subsequently, cell viability was evaluated using the Cell Counting Kit-8 assay, while ferroptosis-related marker levels were determined using biochemical kits, immunofluorescence and western blotting. Activation and homeostasis of the nuclear factor erythroid 2-related factor 2 (Nrf2) signaling pathway were analyzed using western blotting, co-immunoprecipitation and reverse transcription-quantitative PCR. In addition, alterations in renal function parameters and the severity of renal pathological injury in rats were examined. The *in vitro* experiments demonstrated that OB significantly promoted cell viability and inhibited ferroptosis, as evidenced by increased glutathione peroxidase 4 and SLC7A11 expression, and decreased levels of malondialdehyde, ferrous ion and reactive oxygen species ($P<0.05$). Additionally, OB activated the Nrf2 signaling pathway, blocked the interaction between Nrf2 and Kelch-like ECH-associated protein 1, and suppressed Nrf2 ubiquitination and degradation ($P<0.05$). *In vivo*, OB administration improved renal function parameters, including serum creatinine and blood urea nitrogen levels ($P<0.05$), and reduced renal pathological injury, in comparison with the DN group. The results of the present study indicated that OB, a natural small molecule, exhibited significant anti-DN effects, possibly through the regulation of Nrf2 homeostasis to inhibit ferroptosis. Overall, this study provides new evidence for OB as a potential clinical treatment for DN.

Introduction

Due to aging populations, changes in lifestyle and dietary habits, the incidence and prevalence of diabetes have increased over the past few decades. According to the latest Global Burden of Disease study 2021, the prevalence of diabetes among adults in China has risen from 6.1% in 1990 to 12.4% in 2021, with an estimated 114 million people affected; this number is projected to reach ≥174 million by 2050 (1). Diabetic nephropathy (DN), a common and typical microvascular complication of diabetes, affects 20-40% of patients with diabetes (2,3). Hyperglycemia leads to damage to the kidney filtration barrier, resulting in glomerular hyperfiltration, hypertension and a loss of renal tubular epithelial cells. These factors interact and exacerbate each other, leading to persistent proteinuria, progressive kidney injury and ultimately end-stage renal disease (4,5), posing a serious threat to the health and survival of patients with diabetes.

Currently, the management of DN focuses primarily on controlling blood glucose and blood pressure; however, these treatments do not fully prevent renal dysfunction or effectively slow the progression of DN (6). Hemodialysis offers partial renal function replacement but can lead to complications such as hypotension and infection. In addition, although kidney transplant can improve renal function, it is limited by donor shortages and the associated risks of surgery (7). Accordingly, there is an urgent need for novel therapies that are simple, affordable, safe and effective for the treatment of DN.

In previous years, natural compounds, particularly those derived from plants, have attracted significant attention due to their potential therapeutic effects on DN (8,9). Obacunone (OB), a triterpenoid limonoid compound derived from *Citrus* plants, has been shown to exhibit a wide range of pharmacological activities, including anti-inflammatory, anticancer and antioxidant properties (10,11). OB has also demonstrated renal protective effects in various experimental models, as well as antidiabetic properties, such as regulating blood glucose

Correspondence to: Dr Yi Ou, Department of Endocrinology, Shenzhen Fuyong People's Hospital, 181 Daodefeng Road, Fuyong, Baoan, Shenzhen, Guangdong 518100, P.R. China
E-mail: lxx20120904@126.com; huuitti@163.com

Key words: obacunone, diabetic nephropathy, ferroptosis, nuclear factor erythroid 2-related factor 2

levels and ameliorating insulin resistance (12,13). However, the potential of OB in specifically treating DN, a condition characterized by progressive renal damage due to diabetes, remains underexplored.

Therefore, the present study aimed to address the gap in the literature by investigating the therapeutic effects and underlying mechanisms of OB in DN using *in vitro* and *in vivo* models. The findings of the current study may offer novel insights and approaches for the clinical treatment of DN.

Materials and methods

Cell culture and grouping. In the present study, the human renal proximal tubular epithelial cell line HK-2 was used as an *in vitro* model, which was purchased from the American Type Culture Collection. HK-2 cells in the logarithmic phase were cultured at a density of $1x10^5$ cells/ml in Dulbecco's Modified Eagle's Medium (UNIVY Biological Technology) containing 10% fetal bovine serum (Beyotime Institute of Biotechnology) and 1% penicillin/streptomycin solution (Beyotime Institute of Biotechnology) (14). The cells were incubated at 37˚C at 5% CO_2. The glucose concentration in the medium was adjusted to 5.5 mM for the normal culture environment or 30 mM for the high-glucose (HG) environment, as described by Zhou *et al* (15), to mimic the conditions of DN *in vitro*.

Solid OB was purchased from MedChemExpress and was dissolved in 0.5% dimethyl sulfoxide solution to prepare a stock solution, according to the manufacturer's instructions. The stock solution was then diluted with phosphate-buffered saline (PBS) to obtain various concentrations for subsequent experiments.

HK-2 cells were divided into the following five groups: i) Control group: HK-2 cells were cultured in a normal environment for 48 h; ii) HG group: HK-2 cells were cultured in a HG environment for 48 h; iii) HG + OB 20 μM group: HK-2 cells were cultured in a HG environment with 20 μM OB for 48 h; iv) HG + OB 40 μM group: HK-2 cells were cultured in a HG environment with 40 μM OB for 48 h; v) HG + OB 80 μM group: HK-2 cells were cultured in a HG environment with 80 μM OB for 48 h.

Cell Counting Kit-8 (CCK-8) assay. HK-2 cells were seeded into 96-well plates at a density of $1x10^4$ cells/well in 100 μl culture medium and were incubated overnight to allow adherence. To observe the effects of OB on HK-2 cells under normal and HG conditions, various concentrations of OB (0, 5, 10, 20, 40, 80 and 160 μM) were used to treat the cells for 48 h at 37˚C. After treatment, 10 μl CCK-8 solution (cat. no. C0037; Beyotime Institute of Biotechnology) was added to each well. The cells were then incubated at 37˚C for 1 h and the absorbance was measured at 540 nm using a SpectraMax microplate reader (Molecular Devices, LLC) to assess cell viability.

Measurement of malondialdehyde (MDA), glutathione (GSH) and ferrous ion (Fe^{2+}) levels. After treatment, the HK-2 cells from each group seeded in a 6-well plate ($1x10^6$ cells/well) were washed with PBS and harvested via low-speed centrifugation (500 x g, 4˚C, 10 min). The cells were resuspended and disrupted using an ultrasonic cell crusher (Sonics & Materials, Inc.) at 20 kHz and 4˚C for three 10-sec cycles with 10-sec intervals. The supernatant was collected for the assessment of MDA, GSH and Fe^{2+} levels. Following the manufacturer's instructions, the supernatant was mixed and incubated with reagents from the MDA assay kit (cat. no. G4300), GSH assay kit (cat. no. G4305) and Fe^{2+} assay kit (cat. no. G1727) (all from Wuhan Servicebio Technology Co., Ltd.). Finally, MDA levels were determined by measuring the absorbance at 532 nm; GSH levels were assessed by measuring the absorbance at 412 nm; and Fe^{2+} levels were evaluated by measuring the fluorescence intensity at Ex=543 nm/Em=580 nm. The measurements were performed using a SpectraMax multifunctional microplate reader.

Determination of reactive oxygen species (ROS). The fluorescent probe CM-H_2DCFDA (cat. no. HY-D1713; MedChemExpress) was employed to determine intracellular ROS levels. After different treatments, HK-2 cells seeded in confocal cell culture dishes ($1.5x10^6$ cells) were incubated with 10 μM CM-H_2DCFDA solution in the dark at 37˚C for 30 min. Subsequently, images of five random fields from each culture dish were captured under a fluorescence microscope (Olympus Corporation). Fluorescence intensity was quantified using ImageJ (version 1.53; National Institutes of Health), and the average value was taken as the final result.

Western blotting. HK-2 cells were seeded into 6-well plates at a density of $1x10^6$ cells/well and were treated for 48 h. Additionally, rat kidney tissues were collected for protein extraction. Total protein was extracted from both HK-2 cells and rat tissues using radioimmunoprecipitation assay (RIPA) buffer (cat. no. 89901; Thermo Fisher Scientific, Inc.) containing protease and phosphatase inhibitors (cat. no. 78440; Thermo Fisher Scientific, Inc.). For rat tissues, samples were homogenized and centrifuged at 12,000 x g and 4˚C for 15 min to collect the supernatant containing the total protein. For nuclear and cytoplasmic protein extraction from HK-2 cells, the Nuclear and Cytoplasmic Extraction Kit (cat. no. 78833; Thermo Fisher Scientific, Inc.) was used following the manufacturer's instructions. Protein quantification was determined using a bicinchoninic acid protein assay kit (cat. no. ab102536; Abcam). Equal amounts of protein (20 μg/lane) were separated by sodium dodecyl sulfate-polyacrylamide gel electrophoresis (SDS-PAGE) and transferred onto polyvinylidene fluoride membranes (cat. no. 05317; MilliporeSigma). Subsequently, the membranes were blocked with 5% skim milk for 1 h at room temperature, followed by incubation with primary antibodies at 4˚C overnight. The primary antibodies used were as follows: Glutathione peroxidase 4 (GPX4; 1:1,000; cat. no. ab125066), ACSL4 (1:10,000; cat. no. ab155282), SLC7A11 (1:1,000; cat. no. ab307601), ferritin heavy chain 1 (FTH1; 1:1,000; cat. no. ab75972), NQO1 (1:1,000; cat. no. ab28947), heme oxygenase 1 (HO-1; 1:1,000; cat. no. ab68477), nuclear factor erythroid 2-related factor 2 (Nrf2; 1:1,000; cat. no. ab62352), Kelch-like ECH-associated protein 1 (KEAP1; 1:2,000; cat. no. ab119403), β-actin (1:1,000; cat. no. ab8226) and Lamin B1 (1:1,000; cat. no. ab16048) (all from Abcam). Subsequently, the membranes were washed with Tris-buffered saline containing 0.1% Tween 20 and were then incubated with the appropriate HRP-conjugated secondary antibody (1:5,000; cat. no. ab205718, Abcam) for 1 h at room temperature. Protein

bands were visualized using a gel imaging system (Bio-Rad Laboratories, Inc.) and densitometric analysis was performed using ImageJ software (version 1.53). To ensure appropriate protein normalization, β-actin was used as a cytoplasmic loading control, whereas Lamin B1 were used as a nuclear internal loading control.

Reverse transcription-quantitative PCR (RT-qPCR). HK-2 cells were seeded in 6-well plates ($1x10^6$ cells/well) and were treated, after which, total RNA was extracted using TRIzol® reagent (Invitrogen; Thermo Fisher Scientific, Inc.). RNA concentration and purity were assessed using a NanoDrop spectrophotometer (Thermo Fisher Scientific, Inc.). Subsequently, cDNA was synthesized from 1 μg total RNA using the Hifair II First-Strand cDNA Kit (cat. no. 11119ES60; Shanghai Yeasen Biotechnology Co., Ltd.) according to the manufacturer's instructions. qPCR was performed with SYBR Green qPCR Master Mix Kit (cat. no. GK10002; GLPBIO Technology LLC) on the Quant Studio 6 Flex system (Applied Biosystems; Thermo Fisher Scientific, Inc.). The qPCR thermocycling conditions were as follows: 95˚C for 30 sec, followed by 40 cycles at 95˚C for 5 sec and 60˚C for 30 sec. GAPDH was used as the internal control, and gene expression levels were calculated using the $2^{-\Delta\Delta Cq}$ method (16). The primers used for qPCR are shown in Table I.

Co-immunoprecipitation (Co-IP) assay. The interaction between Nrf2 and KEAP1 proteins, as well as the ubiquitination level of Nrf2, was assessed using the Co-IP assay. Briefly, RIPA buffer containing protease and phosphatase inhibitors was added to HK-2 cells from each treatment group. The lysates were centrifuged at 12,000 x g and 4˚C for 15 min, and the supernatants were collected for immunoprecipitation. For each Co-IP reaction, 500 μg total protein lysate was used. Furthermore, 1 μg anti-KEAP1 antibody (cat. no. ab119403; Abcam) was added to the lysate and incubated overnight at 4˚C to capture the KEAP1-Nrf2 complex. The following day, 30 μl protein A/G agarose beads (Shanghai Zeye Biotechnology Co., Ltd.) were added, and the mixture was incubated for 2 h at 4˚C to allow antibody binding. After washing the beads three times with PBS containing 0.1% Tween-20 to remove nonspecific binding, the immunoprecipitated complexes were collected by centrifugation at 3,000 x g and 4˚C for 5 min, resuspended in SDS sample buffer and eluted by boiling at 100˚C for 5 min. Subsequently, the binding of Nrf2 to KEAP1 was detected through SDS-PAGE and western blotting. To detect Nrf2 in the immunoprecipitated complexes, anti-Nrf2 antibody (1:1,000; cat. no. ab62352; Abcam) was used in western blotting. Additionally, to assess Nrf2 ubiquitination, an anti-ubiquitin antibody (1:1,000; cat. no. ab140601; Abcam) was used in western blotting to detect the ubiquitinated Nrf2. IgG negative controls (cat. no. ab171870; Abcam) were included to account for nonspecific binding and to confirm the specificity of the antibody interactions. Due to persistent nonspecific binding despite optimization, IgG negative control and experimental IP samples were analyzed on separate membranes to ensure specificity.

Animal model establishment and grouping. A total of 36 adult healthy specific pathogen-free Sprague-Dawley male rats (age, 8-10 weeks; 180-220 g) were purchased from Beijing Vital River Laboratory Animal Technology Co., Ltd. All animal experiments were conducted at Guangdong Medical Laboratory Animal Center (Guangzhou, China). The laboratory conditions were maintained at 22±1˚C, with a humidity of 45-55%, and under a standard 12-h light/dark cycle. The animals had free access to food and water, and were allowed 1 week of acclimation to the experimental environment. The body weight of the rats was recorded weekly throughout the experimental period to monitor health status and to ensure the successful establishment of the DN model. The present study was approved by the Animal Ethics Committee of Guangdong Medical Laboratory Animal Center (approval no. D202410-3).

Table I. Primers used for quantitative PCR.

Gene	Sequences (5' to 3')
Nrf2	F: 5'-CACGGTCCACAGCTCATCAT-3'
	R: 5'-GCTCATACTCTTTCCGTCGC-3'
KEAP1	F: 5'-AACCGACAACCAAGACCCC-3'
	R: 5'-CTGCATGGGGTTCCAGAAGAT-3'
GAPDH	F: 5'-GGAGCGAGATCCCTCCAAAAT-3'
	R: 5'-GGCTGTTGTCATACTTCTCATGG-3'

F, forward; KEAP1, Kelch-like ECH-associated protein 1; Nrf2, nuclear factor erythroid 2-related factor 2; R, reverse.

Following the method proposed by Xue *et al* (17), streptozotocin (STZ) was used to induce DN. Rats were intraperitoneally injected with STZ (35 mg/kg) to destroy pancreatic β-cells and reduce insulin secretion, combined with a HG and high-fat diet (containing 40% fat, 20% carbohydrates, 20% protein, 5% fiber, 0.5% cholesterol, and additional vitamin and mineral supplements). The Sprague-Dawley rats were randomly divided into the following six experimental groups (n=6/group): Sham group (normal diet), DN group (HG and high-fat diet + STZ injection), DN + OB-L group (HG and high-fat diet + STZ + OB treatment at a low dose of 25 mg/kg), DN + OB-M group (HG and high-fat diet + STZ + OB treatment at a medium dose of 50 mg/kg), DN + OB-H group (HG and high-fat diet + STZ + OB treatment at a high dose of 100 mg/kg) and DN + OB-H + ML385 group (HG and high-fat diet + STZ + OB-H + ML385 treatment).

After 4 weeks of the HG and high-fat diet, rats were fasted for 12-16 h. Rats in the Sham group received an intraperitoneal injection of an equivalent volume of sodium citrate buffer, whereas the rats in the other groups received STZ (35 mg/kg; Sigma-Aldrich; Merck KGaA). The model was considered successful if fasting blood glucose levels exceeded 16.7 mmol/l and 24-h urine output exceeded 150% of normal (18).

Drug and treatment administration. After successful modeling, the rats in the Sham and DN groups received a gavage of an equivalent volume of saline once daily for 8 weeks; whereas rats in the DN + OB-L, DN + OB-M and DN + OB-H, groups received oral gavage administration of OB solution at doses of 25, 50 and 100 mg/kg, respectively, once daily for 8 weeks (19). The rats in the DN + OB-H + ML385 group received an additional intraperitoneal injection of the Nrf2 inhibitor ML385

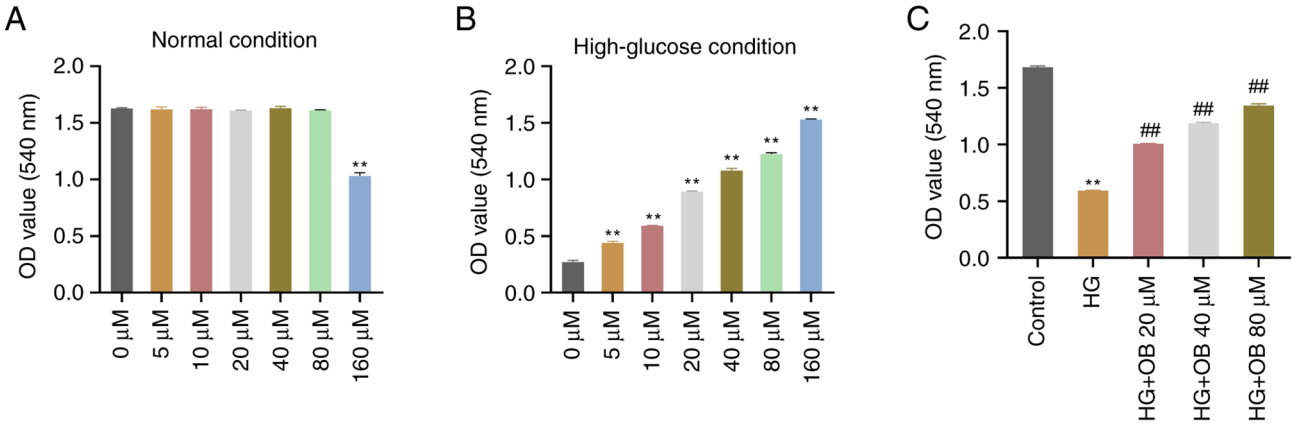

Figure 1. OB reverses the HG-induced inhibition of HK-2 cell viability. CCK-8 assay was used to measure the viability of HK-2 cells under (A) normal conditions or in a (B) HG environment after treatment with OB solutions at different concentrations (0, 5, 10, 20, 40, 80 and 160 μM). Data are presented as the mean ± SD (n=3). **P<0.01 vs. 0 μM. (C) CCK-8 assay was applied to measure the viability of HK-2 cells in the Control, HG, HG + OB 20 μM, HG + OB 40 μM and HG + OB 80 μM groups. Data are presented as the mean ± SD (n=3. **P<0.01 vs. Control group; $^{\#\#}$P<0.01 vs. HG group. CCK-8, Cell Counting Kit-8; HG, high-glucose; OB, obacunone.

(30 μg/kg; Sigma-Aldrich; Merck KGaA) 1 h prior to OB-H treatment, followed by daily oral administration of OB-H (100 mg/kg) for 8 weeks (20).

Sample collection and biochemical analysis. After the 8-week intervention, rats were fasted for 12-16 h and were anesthetized via an intraperitoneal injection of pentobarbital sodium (30 mg/kg). Blood samples were collected via tail vein puncture twice per week, with a volume of 0.3 ml/draw. Additionally, 24-h urine samples were collected to measure total 24-h urinary protein (24 hUP). Rats were euthanized by cervical dislocation while under deep anesthesia with pentobarbital sodium to ensure humane treatment. The kidneys were immediately harvested, weighed and processed for further analysis. The kidney weight-to-body weight ratio was calculated as the kidney index.

Blood samples were centrifuged at 1,000 x g for 10 min at 4˚C to collect the supernatant, and blood urea nitrogen (BUN; cat. no. EIABUN; Invitrogen; Thermo Fisher Scientific, Inc.) and creatinine (Cr; cat. no. EIASCR; Invitrogen; Thermo Fisher Scientific, Inc.) levels were measured using commercial kits according to the manufacturer's protocols. For kidney biochemical analysis, the left kidney tissue was cut into 1-2 mm^3 pieces, homogenized in PBS buffer using a homogenizer and was centrifuged at 10,000 x g for 15 min at 4˚C. The supernatant was collected for the measurement of MDA (cat. no. G4302; Wuhan Servicebio Technology Co., Ltd.) and GSH (cat. no. G4305; Wuhan Servicebio Technology Co., Ltd.) levels according to the manufacturer's protocols. Protein extraction was performed using RIPA buffer containing protease and phosphatase inhibitors, and the protein levels of GPX4, ACSL4, SLC7A11 and FTH1 were detected by western blotting as aforementioned.

Hematoxylin and eosin (H&E) staining. The right kidney was fixed in 10% formalin at room temperature for 24 h, dehydrated, embedded in paraffin and sectioned into 5-μm slices (21). After deparaffinization and rehydration, the sections were stained with hematoxylin for 10 min and eosin for 3 min at room temperature. Five random fields of view from each kidney section were selected and examined under a light microscope to assess pathological changes.

Statistical analysis. Data are presented as the mean ± SD and each experiment was independently repeated at least three times per group. Statistical analyses were carried out using SPSS 22.0 software (IBM Corp.). Data were tested for normality using the Shapiro-Wilk test and for homogeneity of variances using Levene's test. For normally distributed data with equal variances, one-way analysis of variance was performed, followed by Tukey's test for post hoc pairwise comparisons. If variances were unequal, Dunnett T3 test was applied for post hoc analysis. P<0.05 was considered to indicate a statistically significant difference.

Results

OB reverses the HG-induced inhibition of HK-2 cell viability. To investigate the effects of OB on HK-2 cell viability under both normal and HG conditions, cells were treated with different concentrations of OB. The CCK-8 assay indicated that no significant differences in cell viability were observed in HK-2 cells treated with 0-80 μM OB under normal conditions (P>0.05); however, treatment with 160 μM OB significantly reduced cell viability compared with that in the 0 μM group (P=0.002; Fig. 1A). Under HG conditions, OB treatment significantly increased cell viability in a dose-dependent manner, with significant differences at all concentrations compared with the Control (all P<0.01; Fig. 1B). These results indicated that OB promoted HK-2 cell viability under HG conditions but was cytotoxic at higher concentrations under normal conditions. Therefore, OB concentrations of 20, 40 and 80 μM were selected for subsequent experiments.

Renal tubular epithelial cells initiate a repair mechanism in response to kidney damage, re-entering the cell cycle and proliferating to replace damaged cells (22). The CCK-8 assay showed that cell viability in the HG group was significantly reduced compared with that in the Control group (P<0.01; Fig. 1C). By contrast, treatment with OB significantly increased

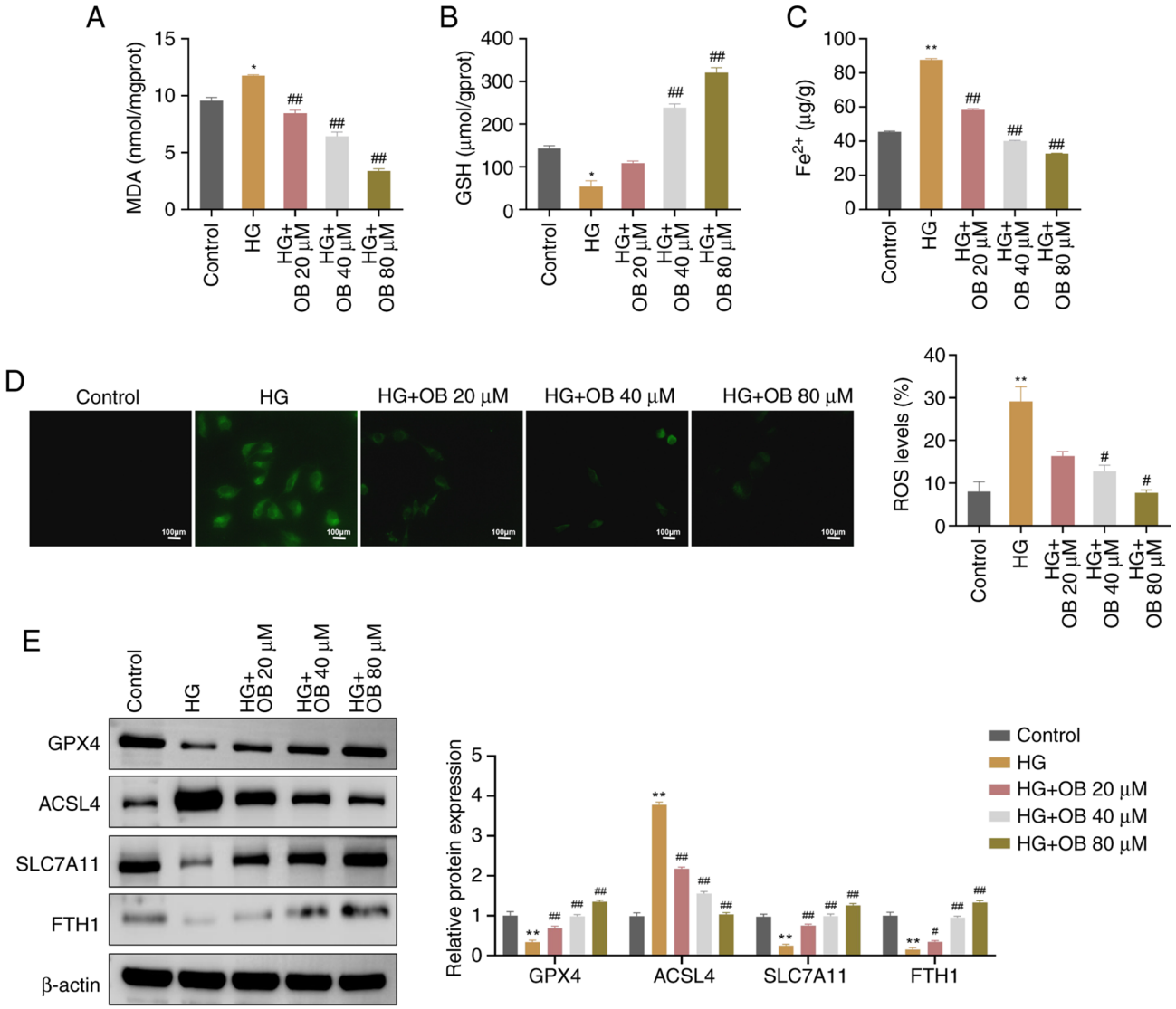

Figure 2. OB inhibits HG-induced ferroptosis in HK-2 cells. The levels of (A) MDA, (B) GSH and (C) Fe^{2}□ in HK-2 cells from the Control, HG, HG + OB 20 μM, HG + OB 40 μM and HG + OB 80 μM groups were measured using biochemical assay kits. (D) Levels of ROS in HK-2 cells from each group were measured using immunofluorescence. (E) Protein levels of GPX4, ACSL4, SLC7A11 and FTH1 in HK-2 cells from each group were measured using western blotting. Data are presented as the mean ± SD (n=3). *P<0.05, **P<0.01 vs. Control group; $^{\#}$P<0.05, $^{\#\#}$P<0.01 vs. HG group. Fe^{2+}, ferrous ion; FTH1, ferritin heavy chain 1; GSH, glutathione; GPX4, glutathione peroxidase 4; HG, high-glucose; MDA, malondialdehyde; OB, obacunone; ROS, reactive oxygen species.

cell viability in a concentration-dependent manner (80 μM: P<0.01), with higher OB concentrations yielding greater cell viability (Fig. 1C). These results suggested that OB effectively reversed the HG-induced inhibition of HK-2 cell viability.

OB inhibits HG-induced ferroptosis in HK-2 cells. The present study next examined whether OB improved HK-2 cell viability by inhibiting ferroptosis. In the HG environment, the levels of MDA (P=0.011) and Fe^{2}□ (P<0.01) were significantly elevated, whereas GSH levels were significantly reduced (P=0.011) compared with those in the Control group (Fig. 2A-C). Treatment with OB significantly reduced MDA (80 μM: P<0.01) and Fe^{2}□ levels (P<0.01), and increased GSH levels (P<0.01), with these effects being concentration-dependent (Fig. 2A-C).

Additionally, immunofluorescence analysis demonstrated that ROS fluorescence intensity was significantly higher in the HG group (P<0.01), and was significantly decreased in response to OB treatment (80 μM: P=0.027) in a dose-dependent manner (Fig. 2D).

Western blot analysis of ferroptosis-related proteins revealed that GPX4 (P=0.009), SLC7A11 (P=0.002) and FTH1 (P=0.003) were significantly decreased, whereas ACSL4 (P<0.01) were significantly increased in the HG group compared with those in the Control group (Fig. 2E). By contrast, treatment with OB reversed these changes in a concentration-dependent manner (GPX4: P<0.01; SLC7A11: P<0.01; FTH1: P<0.01; ACSL4: P<0.01 for 80 μM; Fig. 2E). Collectively, these results indicated that OB could inhibit HG-induced ferroptosis in HK-2 cells.

OB activates the Nrf2 signaling pathway in HK-2 cells under HG conditions. Nrf2 activation is known to protect cells against oxidative stress and ferroptosis (23). The present study explored whether OB exerts its protective effects by activating the Nrf2 signaling pathway. Western blot analysis showed that

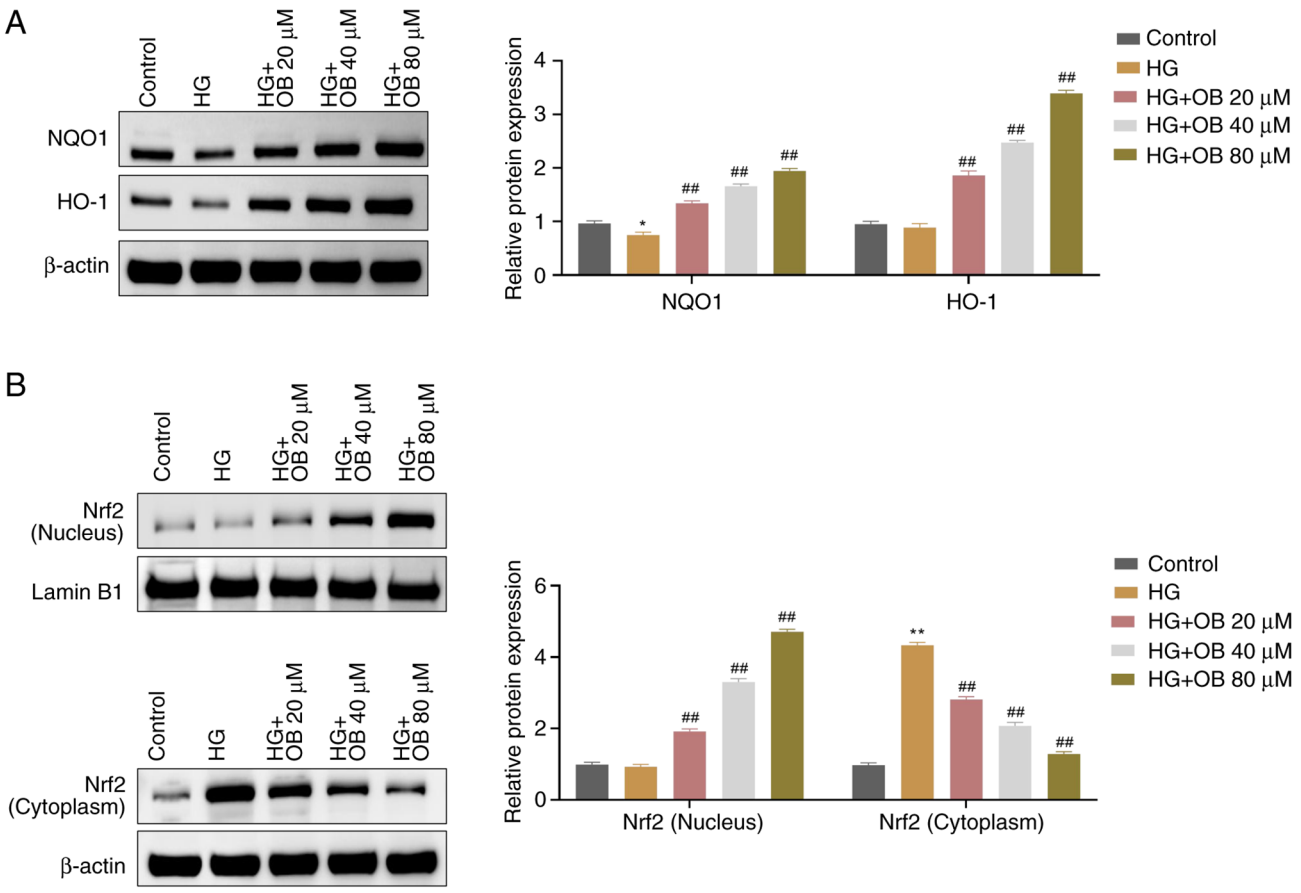

Figure 3. OB activates the Nrf2 signaling pathway in HK-2 cells under HG conditions. (A) Western blotting was conducted to evaluate the protein levels of NQO1 and HO-1 in HK-2 cells from the Control, HG, HG + OB 20 μM, HG + OB 40 μM and HG + OB 80 μM groups. (B) Western blotting was applied to assess the protein levels of Nrf2 in the cytoplasm and nucleus of HK-2 cells. Data are presented as the mean ± SD (n=3). *P<0.05, **P<0.01 vs. Control group; $^{\#\#}$P<0.01 vs. HG group. HG, high-glucose; HO-1, heme oxygenase 1; Nrf2, nuclear factor erythroid 2-related factor 2 ; OB, obacunone.

the levels of NQO1 were significantly reduced in the HG group compared with those in the Control group (P=0.031), whereas the protein levels of HO-1 were slightly decreased without statistical significance (P=0.895) (Fig. 3A). Compared with those in the HG group, the levels of NQO1 (80 μM: P<0.01) and HO-1 (80 μM: P<0.01) were significantly increased in the OB treatment groups, in a dose-dependent manner (Fig. 3A). Additionally, in the HG group, cytoplasmic Nrf2 levels were significantly increased (P<0.01), while nuclear Nrf2 levels were not significantly different (P=0.931), compared with those in the Control group (Fig. 3B). OB treatment resulted in significantly lower cytoplasmic Nrf2 levels (80 μM: P<0.01) and significantly higher nuclear Nrf2 levels (80 μM: P<0.01) in a dose-dependent manner (Fig. 3B). These results suggested that OB could activate the Nrf2 signaling pathway under HG conditions.

OB suppresses the ubiquitination and degradation of Nrf2 by blocking its interaction with KEAP1. To investigate how OB regulates Nrf2, the current study assessed the interaction between Nrf2 and KEAP1, and the ubiquitination level of Nrf2. RT-qPCR results indicated that Nrf2 expression levels were significantly lower in the HG group (P=0.001) and KEAP1 levels were significantly higher (P<0.01), compared with those in the Control group; however, treatment with OB did not reverse the expression of Nrf2 (all P>0.05) or KEAP1 (all P>0.05) (Fig. 4A and B). Western blot analysis revealed that there were no significant changes in KEAP1 protein levels across the groups (all P>0.05; Fig. 4C). However, the interaction between Nrf2 and KEAP1 was significantly enhanced in the HG group (P<0.01) compared with that in the Control group; by contrast, OB treatment significantly reduced the Nrf2-KEAP1 interaction in a concentration-dependent manner (80 μM: P<0.01) (Fig. 4D). Additionally, the ubiquitination level of Nrf2 was significantly increased in the HG group (P<0.001) compared with that in the Control group and was significantly decreased in the OB treatment groups (80 μM: P<0.01) (Fig. 4E). These results suggested that OB may inhibit the interaction between Nrf2 and KEAP1, preventing Nrf2 degradation and promoting its nuclear translocation.

OB mitigates DN in vivo by inhibiting ferroptosis. To further validate the *in vitro* findings, the present study assessed the effects of OB on a rat model of DN. Compared with in the Sham group, the DN group exhibited significantly elevated levels of BUN (P=0.001), Cr (P=0.001), 24 hUP (P=0.001) and renal index (P<0.01) (Fig. 5A-D). By contrast, treatment with OB significantly reduced these parameters in a dose-dependent manner (BUN: P<0.01; Cr: P<0.01; 24 hUP: P=0.001; renal index: P=0.001 for 100 mg/kg). Conversely, co-administration of the Nrf2 inhibitor ML385 reversed the beneficial effects of OB, resulting in significantly elevated BUN (P<0.01), Cr

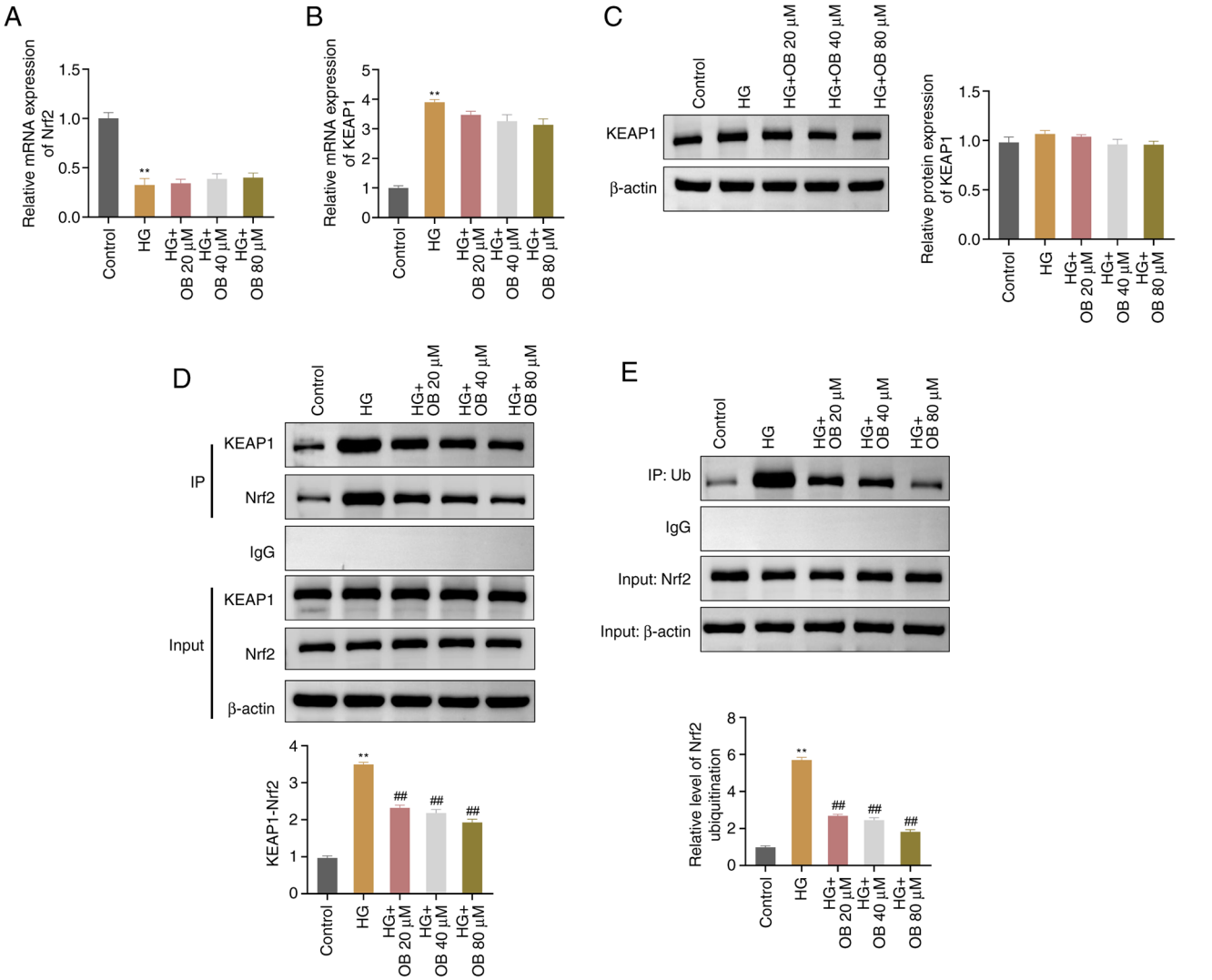

Figure 4. OB blocks the ubiquitination and degradation of Nrf2 by blocking its interaction with KEAP1 under HG conditions. The expression levels of (A) Nrf2 and (B) KEAP1 in HK-2 cells from the Control, HG, HG + OB 20 μM, HG + OB 40 μM and HG + OB 80 μM groups were assessed using reverse transcription-quantitative PCR. (C) KEAP1 protein levels in HK-2 cells from each group were detected by western blotting. (D) Interaction between Nrf2 and KEAP1 in HK-2 cells from all groups was assessed using the Co-IP assay. (E) Ubiquitination of Nrf2 in HK-2 cells from each group was evaluated using the Co-IP assay. Data are presented as the mean ± SD (n=3). **P<0.01 vs. Control group; $^{\#\#}$P<0.01 vs. HG group. HG, high-glucose; KEAP1, Kelch-like ECH-associated protein 1; Nrf2, nuclear factor erythroid 2-related factor 2; OB, obacunone; Co-IP, co-immunoprecipitation.

(P=0.004), 24 hUP (P=0.001) and renal index (P=0.017) compared with in the DN + OB-H group (Fig. 5A-D).

Histological analysis showed improved renal pathology in the OB treatment groups, with decreased glomerular volume and tubular dilation compared with in the DN group (Fig. 5E). However, the DN + OB-H + ML385 group exhibited aggravated renal injury compared with the DN + OB-H group, suggesting that the protective effects of OB were dependent on Nrf2 activation. This was consistent with the *in vitro* results, where OB enhanced HK-2 cell viability under HG conditions, further supporting its protective role (Fig. 5E).

In terms of oxidative stress, the DN group exhibited significantly higher MDA levels (P=0.004) and lower GSH levels (P=0.049) compared with those in the Sham group (Fig. 5F). By contrast, OB treatment significantly reduced MDA levels (P<0.01) and increased GSH levels (P=0.002) in a concentration-dependent manner. Notably, the DN + OB-H + ML385 group showed significantly higher MDA levels (P=0.024) and lower GSH levels (P<0.01) compared with in the DN + OB-H group (Fig. 5F).

Western blot analysis revealed that the levels of GPX4 (P<0.01), SLC7A11 (P<0.01) and FTH1 (P=0.008) were significantly reduced in the DN group compared with those in the Sham group, whereas ACSL4 levels were significantly elevated (P<0.01) (Fig. 5G). By contrast, OB treatment significantly reversed the expression levels of these proteins (GPX4: P=0.004; SLC7A11: P=0.002; FTH1: P=0.008; ACSL4: P<0.01 for 100 mg/kg). Notably, the DN + OB-H + ML385 group showed diminished expression of GPX4 (P=0.03), SLC7A11 (P<0.01) and FTH1 (P=0.015), and an increase in ACSL4 (P<0.01) compared with those in the DN + OB-H group (Fig. 5G).

Collectively, these findings suggested that OB could significantly alleviate DN *in vivo* by modulating oxidative stress and inhibiting ferroptosis. However, the effect was partially attenuated by the Nrf2 inhibitor ML385, indicating that OB

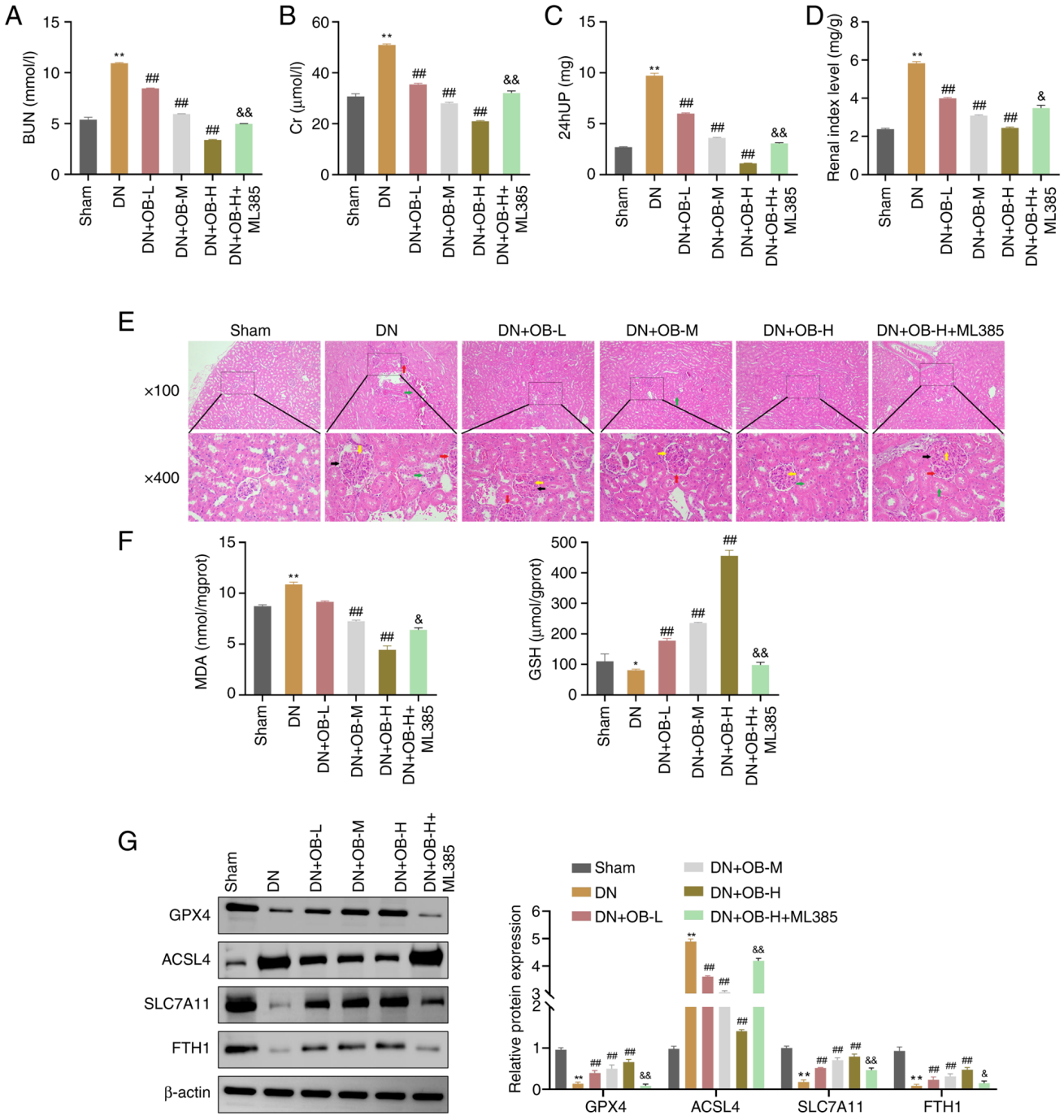

Figure 5. OB exerts its anti-DN functions *in vivo* through suppressing ferroptosis. (A) Serum BUN, (B) serum Cr and (C) 24 hUP levels were assessed in rats from each group. (D) Renal index was determined for rats in each group. (E) Severity of renal pathological damage in each group of rats was observed using hematoxylin and eosin staining (red arrow: glomerular hypertrophy; green arrow: mesangial expansion; yellow arrow: thickening of the glomerular basement membrane; black arrow: tubular dilation with epithelial detachment). (F) Levels of MDA and GSH in renal tissues were measured using biochemical assay kits (G) Protein levels of GPX4, ACSL4, SLC7A11 and FTH1 in renal tissues were assessed by western blotting. Data are presented as the mean ± SD (n=3). *P<0.05, **P<0.01 vs. Sham group; $^{\#\#}$P<0.01 vs. DN group; $^{\&}$P<0.05, $^{\&\&}$P<0.01 vs. DN + OB-H group. 24 hUP, 24-h urinary protein; BUN, blood urea nitrogen; Cr, creatinine; DN, diabetic nephropathy; FTH1, ferritin heavy chain 1; GPX4, glutathione peroxidase 4; GSH, glutathione; MDA, malondialdehyde; OB, obacunone.

might exert its protective effects by enhancing Nrf2 signaling, thereby mitigating oxidative stress-induced ferroptosis in DN.

Discussion

The present study demonstrated that OB exhibited significant anti-DN effects in *in vitro* and *in vivo* models. Mechanistically, the effects of OB may be attributed to its ability to inhibit ferroptosis in renal tubular epithelial cells by regulating Nrf2 homeostasis. The current study provides valuable insights into the renal protective effects of OB, highlighting its potential as a therapeutic agent for DN. By systematically exploring the protective effects and underlying mechanisms, this study lays a strong foundation for the potential clinical application in DN treatment.

There is substantial theoretical justification for selecting OB as a potential treatment for DN in the present study. Previous research has demonstrated that OB protects renal function and exhibits significant anti-diabetic properties (12,13). DN is a progressive renal disease triggered by a HG environment, and OB has been shown to improve this disease (15), which is consistent with the results of the present study. In addition, pharmacokinetic studies have verified that OB is mainly metabolized in the liver, and renal metabolism or excretion does not occur (10). This significantly reduces the burden on the kidneys and lowers the risk of drug-induced renal damage, suggesting the suitability of OB for treating DN without exacerbating renal injury.

The present study established both *in vitro* cell models and *in vivo* animal models to comprehensively elucidate the pharmacological effects of OB. *In vitro*, HK-2 cells were exposed to 30 mM glucose to simulate the nephrotoxicity caused by a HG environment, closely mimicking the pathophysiological conditions of DN. The experimental results revealed that the viability of HK-2 cells was significantly reduced after exposure to HG, confirming the successful construction of the cell model. Similarly, in the *in vivo* model, DN was induced in rats by feeding them a HG and high-fat diet, and administering STZ intraperitoneally. The model exhibited significantly elevated levels of 24 hUP, BUN and Cr, indicating impaired renal function, and the typical pathological changes of DN, such as enlarged glomerular volume and abnormal tubular morphology (24), further validating the success of the animal model.

To verify the renal protective effect of OB, its impact was first assessed on the viability of HK-2 cells. Renal tubular epithelial cells serve essential roles in reabsorbing electrolytes and water, and regulating acid-base balance in the body. A sufficient number of renal tubular epithelial cells is crucial for maintaining kidney function and structure (25). The present results indicated that OB effectively reversed the HG-induced inhibition of HK-2 cell viability, providing preliminary evidence of its anti-DN effects. *In vivo*, OB improved renal function and pathological damage in rats with DN, further supporting this conclusion.

After confirming the efficacy of OB in DN, the present study further assessed its underlying mechanism. Ferroptosis, a form of programmed cell death characterized by lipid peroxides and iron dysregulation, has been linked to the pathogenesis of DN. Under normal conditions, SLC7A11 and GPX4 promote the synthesis of GSH, protecting cells from oxidative stress (26); however, during ferroptosis, the reduction of GPX4 and SLC7A11 leads to decreased GSH synthesis, ROS accumulation and iron overload, which promotes oxidative damage and lipid peroxidation, culminating in cell death (27,28). The present study demonstrated that after OB intervention, the levels of ROS, MDA, Fe^{2+} and ACSL4 were significantly reduced, whereas GSH, GPX4, SLC7A11 and FTH1 were increased, suggesting that OB may exert its effects by inhibiting ferroptosis. This mechanism is consistent with that observed in natural compounds such as ginkgolide B, *Hibiscus sabdariffa* and chicoric acid, which also utilize antioxidant-rich pathways to combat DN (29-31).

Oxidative stress has a key role in ferroptosis and maintaining intracellular redox balance is essential to inhibit ferroptosis (32). Given the ability of OB to regulate oxidative stress and ferroptosis, the current study focused on its effects on Nrf2, a key transcription factor involved in oxidative stress responses. Under normal conditions, Nrf2 is bound to KEAP1, forming an inactive complex that is targeted for ubiquitination and degradation. However, when oxidative stress is triggered, the Nrf2-KEAP1 interaction weakens, leading to the translocation of Nrf2 into the nucleus, where it activates the expression of downstream antioxidant genes, such as HO-1 and NQO1 (33). The present results showed that OB inhibited Nrf2 ubiquitination and facilitated its nuclear translocation, leading to the increased expression of NQO1 and HO-1, which in turn suppressed oxidative damage and ferroptosis. These findings align with those of previous studies demonstrating that OB activates the Nrf2 pathway to alleviate inflammatory pain, acute lung injury and liver fibrosis (34-36). Furthermore, the findings of the current study extend the work of Zhou *et al* (15); this previous study demonstrated that OB can attenuate HG-induced oxidative stress in NRK-52E cells via GSK-3β inhibition. The present study revealed an additional mechanism through the Nrf2 pathway, highlighting the dual role of OB in mitigating oxidative stress and ferroptosis, which indicates a novel therapeutic strategy for DN.

It is worth noting that the clinical application of OB in treating DN requires careful consideration of blood glucose levels. The present results indicated that OB primarily enhanced the viability of HK-2 cells under HG conditions, but did not show the same effect under normal conditions. This result suggested that OB is particularly effective in DN, and may have limited efficacy for other types of kidney diseases, such as autoimmune-mediated nephritis (37), or acute kidney injury caused by ischemia or nonsteroidal anti-inflammatory drugs (38,39).

Notably, there are some limitations in the present study. Firstly, the typical morphological features of ferroptosis, such as mitochondrial rupture or membrane perforation, were not directly observed using transmission electron microscopy. Secondly, the relatively short observation period in the *in vivo* experiments limited the ability to evaluate the long-term safety and efficacy of OB. Future studies should extend the observation period to assess the long-term effects of OB treatment on renal function, and potential drug resistance or side effects. Additionally, exploring the effects of OB on other tissues, such as the heart or nervous system, would be valuable in determining its broader therapeutic potential for other diabetic complications. Moreover, while a rat model was used to evaluate the effects of OB on DN, the lack of a humanized kidney model may limit the translational relevance of the present findings. Future studies should consider constructing rat models with humanized kidneys to better simulate human DN and to improve the clinical applicability of the results.

Another important consideration is that excessively high concentrations of OB could potentially induce cytotoxicity. The exact mechanisms underlying this toxicity are not fully understood and require further investigation. Future studies should focus on elucidating the molecular mechanisms, such as oxidative stress, mitochondrial dysfunction and inflammatory

pathways, that contribute to OB-induced toxicity at high doses. In addition, toxicological studies using dose-response models and long-term *in vivo* studies will help establish the safe therapeutic range for OB and clarify its long-term safety profile. Notably, due to persistent nonspecific binding observed in the co-IP experiments, IgG negative control and experimental IP samples were analyzed on separate membranes to ensure specificity. While this minimized cross-reactivity, it may limit direct comparability, warranting further optimization in future studies.

In conclusion, the present results demonstrated that the natural small molecule OB had notable anti-DN effects in both *in vitro* and *in vivo* models. The effects of OB on DN were possibly achieved through the inhibition of ferroptosis in renal tubular epithelial cells by regulating Nrf2 homeostasis. Overall, the current study revealed the potential value of OB in DN intervention and provided a new therapeutic option for the clinical treatment of DN.

Acknowledgements

Not applicable.

Funding

No funding was received.

Availability of data and materials

The data generated in the present study may be requested from the corresponding author.

Authors' contributions

YO conceptualized the study and designed the methodology. Formal analysis was conducted by YO and WJZ. Data curation was performed by WJZ. YO drafted the original manuscript, and both YO and WJZ contributed to the writing, review and editing. WJZ was responsible for project administration, supervision and investigation. Validation was carried out by both YO and WJZ. Both authors confirm the authenticity of all the raw data, and have read and approved the final version of the manuscript.

Ethics approval and consent to participate

The experiment was conducted in strict accordance with The Guide for the Care and Use of Laboratory Animals to ensure animal welfare. Since Shenzhen Fuyong People's Hospital does not have an Animal Ethics Committee, the study was reviewed and approved by the Animal Ethics Committee of Guangdong Medical Laboratory Animal Center (approval no. D202410-3).

Patient consent for publication

Not applicable.

Competing interests

The authors declare that they have no competing interests.

References

1. Deng W, Zhao L, Chen C, Ren Z, Jing Y, Qiu J and Liu D: National burden and risk factors of diabetes mellitus in China from 1990 to 2021: Results from the Global Burden of Disease study 2021. J Diabetes 16: e70012, 2024.
2. Qi C, Mao X, Zhang Z and Wu H: Classification and differential diagnosis of diabetic nephropathy. J Diabetes Res 2017: 8637138, 2017.
3. Kanaley JA, Colberg SR, Corcoran MH, Malin SK, Rodriguez NR, Crespo CJ, Kirwan JP and Zierath JR: Exercise/physical activity in individuals with type 2 diabetes: A consensus statement from the American college of sports medicine. Med Sci Sports Exerc 54: 353-368, 2022.
4. Chen J, Liu Q, He J and Li Y: Immune responses in diabetic nephropathy: Pathogenic mechanisms and therapeutic target. Front Immunol 13: 958790, 2022.
5. Zoja C, Xinaris C and Macconi D: Diabetic nephropathy: Novel molecular mechanisms and therapeutic targets. Front Pharmacol 11: 586892, 2020.
6. Naaman SC and Bakris GL: Diabetic nephropathy: Update on pillars of therapy slowing progression. Diabetes Care 46: 1574-1586, 2023.
7. Samsu N: Diabetic nephropathy: Challenges in pathogenesis, diagnosis, and treatment. Biomed Res Int 2021: 1497449, 2021.
8. Zhou TY, Tian N, Li L and Yu R: Iridoids modulate inflammation in diabetic kidney disease: A review. J Integr Med 22: 210-222, 2024.
9. Shinjyo N, Parkinson J, Bell J, Katsuno T and Bligh A: Berberine for prevention of dementia associated with diabetes and its comorbidities: A systematic review. J Integr Med 18: 125-151, 2020.
10. Zheng W, Yang S and Chen X: The pharmacological and pharmacokinetic properties of obacunone from citrus fruits: A comprehensive narrative review. Fitoterapia 169: 105569, 2023.
11. Wang S, Kuperman LL, Song Z, Chen Y, Liu K, Xia Z, Xu Y and Yu Q: An overview of limonoid synthetic derivatives as promising bioactive molecules. Eur J Med Chem 259: 115704, 2023.
12. Ono E, Inoue J, Hashidume T, Shimizu M and Sato R: Anti-obesity and anti-hyperglycemic effects of the dietary citrus limonoid nomilin in mice fed a high-fat diet. Biochem Biophys Res Commun 410: 677-681, 2011.
13. Qiu Z, He J, Shao G, Hu J, Li X, Zhou H, Li M and Yang B: Obacunone retards renal cyst development in autosomal dominant polycystic kidney disease by activating NRF2. Antioxidants (Basel) 11: 38, 2021.
14. Kurosaki Y, Imoto A, Kawakami F, Ouchi M, Morita A, Yokoba M, Takenaka T, Ichikawa T, Katagiri M, Nielsen R and Ishii N: In vitro study on effect of bardoxolone methyl on cisplatin-induced cellular senescence in human proximal tubular cells. Mol Cell Biochem 477: 689-699, 2022.
15. Zhou J, Wang T, Wang H, Jiang Y and Peng S: Obacunone attenuates high glucose-induced oxidative damage in NRK-52E cells by inhibiting the activity of GSK-3beta. Biochem Biophys Res Commun 513: 226-233, 2019.
16. Livak KJ and Schmittgen TD: Analysis of relative gene expression data using real-time quantitative PCR and the 2(-Delta Delta C(T)) method. Methods 25: 402-408, 2001.
17. Xue S, Li YX, Lu XX and Tang W: Dapagliflozin can alleviate renal fibrosis in rats with streptozotocin-induced type 2 diabetes mellitus. Exp Ther Med 26: 572, 2023.
18. Wahab NAA, Giribabu N, Kilari EK and Salleh N: Abietic acid ameliorates nephropathy progression via mitigating renal oxidative stress, inflammation, fibrosis and apoptosis in high fat diet and low dose streptozotocin-induced diabetic rats. Phytomedicine 107: 154464, 2022.
19. Lang X, Zhang X, Wang D and Zhou W: In vitro and in vivo metabolic activation of obacunone, a bioactive and potentially hepatotoxic constituent of dictamni cortex. Planta Med 86: 686-695, 2020.
20. AlTamimi JZ, AlFaris NA, Alshammari GM, Alagal RI, Aljabryn DH and Abdo Yahya M: Protective effect of eriodictyol against hyperglycemia-induced diabetic nephropathy in rats entails antioxidant and anti-inflammatory effects mediated by activating Nrf2. Saudi Pharm J 31: 101817, 2023.
21. Fischer AH, Jacobson KA, Rose J and Zeller R: Hematoxylin and eosin staining of tissue and cell sections. CSH Protoc 2008: pdb prot4986, 2008.

22. Liu Y and Tang SC: Recent progress in stem cell therapy for diabetic nephropathy. Kidney Dis (Basel) 2: 20-27, 2016.
23. Song X and Long D: Nrf2 and Ferroptosis: A new research direction for neurodegenerative diseases. Front Neurosci 14: 267, 2020.
24. Sharma K, McCue P and Dunn SR: Diabetic kidney disease in the db/db mouse. Am J Physiol Renal Physiol 284: F1138-F1144, 2003.
25. Li Z, Lu S and Li X: The role of metabolic reprogramming in tubular epithelial cells during the progression of acute kidney injury. Cell Mol Life Sci 78: 5731-5741, 2021.
26. Stockwell BR, Friedmann Angeli JP, Bayir H, Bush AI, Conrad M, Dixon SJ, Fulda S, Gascón S, Hatzios SK, Kagan VE, *et al*: Ferroptosis: A regulated cell death nexus linking metabolism, redox biology, and disease. Cell 171: 273-285, 2017.
27. Ding K, Liu C, Li L, Yang M, Jiang N, Luo S and Sun L: Acyl-CoA synthase ACSL4: an essential target in ferroptosis and fatty acid metabolism. Chin Med J (Engl) 136: 2521-2537, 2023.
28. Mengstie MA, Seid MA, Gebeyehu NA, Adella GA, Kassie GA, Bayih WA, Gesese MM, Anley DT, Feleke SF, Zemene MA, *et al*: Ferroptosis in diabetic nephropathy: Mechanisms and therapeutic implications. Metabol Open 18: 100243, 2023.
29. Chen J, Ou Z, Gao T, Yang Y, Shu A, Xu H, Chen Y and Lv Z: Ginkgolide B alleviates oxidative stress and ferroptosis by inhibiting GPX4 ubiquitination to improve diabetic nephropathy. Biomed Pharmacother 156: 113953, 2022.
30. Ajiboye BO, Famusiwa CD, Nifemi DM, Ayodele BM, Akinlolu OS, Fatoki TH, Ezzat AO, Al-Lohedan HA, Gupta S and Oyinloye BE: Nephroprotective effect of hibiscus sabdariffa leaf flavonoid extracts via KIM-1 and TGF-1beta signaling pathways in streptozotocin-induced rats. ACS Omega 9: 19334-19344, 2024.
31. Zhang W, Liu Y, Zhou J, Qiu T, Xie H and Pu Z: Chicoric acid advanced PAQR3 ubiquitination to ameliorate ferroptosis in diabetes nephropathy through the relieving of the interaction between PAQR3 and P110alpha pathway. Clin Exp Hypertens 46: 2326021, 2024.
32. Jiang X, Stockwell BR and Conrad M: Ferroptosis: mechanisms, biology and role in disease. Nat Rev Mol Cell Biol 22: 266-282, 2021.
33. Chen F, Xiao M, Hu S and Wang M: Keap1-Nrf2 pathway: A key mechanism in the occurrence and development of cancer. Front Oncol 14: 1381467, 2024.
34. Nan F, Tian Q and Chen S: Obacunone alleviates inflammatory pain by promoting m2 microglial polarization and by activating Nrf2/HO-1 signaling pathway. Drug Des Devel Ther 18: 1265-1275, 2024.
35. Li J, Deng SH, Li J, Li L, Zhang F, Zou Y, Wu DM and Xu Y: Obacunone alleviates ferroptosis during lipopolysaccharide-induced acute lung injury by upregulating Nrf2-dependent antioxidant responses. Cell Mol Biol Lett 27: 29, 2022.
36. Bai Y, Wang W, Wang L, Ma L, Zhai D, Wang F, Shi R, Liu C, Xu Q, Chen G and Lu Z: Obacunone attenuates liver fibrosis with enhancing anti-oxidant effects of GPx-4 and inhibition of EMT. Molecules 26: 318, 2021.
37. Anders HJ and Schlondorff D: Toll-like receptors: Emerging concepts in kidney disease. Curr Opin Nephrol Hypertens 16: 177-183, 2007.
38. Bonventre JV and Yang L: Cellular pathophysiology of ischemic acute kidney injury. J Clin Invest 121: 4210-4221, 2011.
39. Zhang X, Donnan PT, Bell S and Guthrie B: Non-steroidal anti-inflammatory drug induced acute kidney injury in the community dwelling general population and people with chronic kidney disease: Systematic review and meta-analysis. BMC Nephrol 18: 256, 2017.